Physica Scripta

INCLUSIVE PUBLISHING TRUSTED SCIENCE

PURPOSE-LED PUBLISHING™

PAPER • **OPEN ACCESS**

Broadband optical response of layered $TlGaSe_2$ from the near-infrared to the ultraviolet: pseudo-optical parameters and vibrational properties

To cite this article: Giray Mecit *et al* 2026 *Phys. Scr.* **101** 385907

View the article online for updates and enhancements.

You may also like

- Linearized Augmented Plane Wave Band Structure Calculations and Dielectric Function of Layered $TlGaSe_2$
Guseyn Orudzhev, YongGu Shim, Kazuki Wakita et al.
- Origin of the optical absorption of $TlGaSe_2$ layered semiconductor in the visible range
Asuman Cengiz, Yurii M Chumakov, Mehmet Erdem et al.
- Electrical and Optical Properties of $TlGaSe_2$ and $TlGaSe_2$:Co Single Crystals
Chang-Sun Yoon, Byong-Ho Kim, Duk-Joon Cha et al.

This content was downloaded from IP address 144.122.201.61 on 28/09/2026 at 17:07

Physica Scripta

Check for updates

OPEN ACCESS

RECEIVED
6 August 2026

REVISED
31 August 2026

ACCEPTED FOR PUBLICATION
11 September 2026

PUBLISHED
21 September 2026

Original content from this work may be used under the terms of the Creative Commons Attribution 4.0 licence.

Any further distribution of this work must maintain attribution to the author(s) and the title of the work, journal citation and DOI.

PAPER

Broadband optical response of layered $TlGaSe_2$ from the near-infrared to the ultraviolet: pseudo-optical parameters and vibrational properties

Giray Mecit[1,2,*], **Mehmet Isik**[3], **Cansu Corapci**[3] and **Nizami Gasanly**[2,4]

[1] Basic Sciences, TED University, Ankara 06420, Türkiye
[2] Department of Physics, Middle East Technical University, Ankara 06800, Türkiye
[3] Department of Biomedical Engineering, Faculty of Engineering and Architecture, İzmir Bakırçay University, İzmir 35665, Türkiye
[4] Virtual International Scientific Research Centre, Baku State University, Baku 1148, Azerbaijan
[*] Author to whom any correspondence should be addressed.

E-mail: giray.mecit@tedu.edu.tr

Keywords: $TlGaSe_2$, layered semiconductor, spectroscopic ellipsometry, pseudo-optical constants, band gap, Raman scattering, optoelectronic materials

Abstract

The broadband optical response of layered $TlGaSe_2$ single crystals was investigated at room temperature by spectroscopic ellipsometry over the photon-energy range of 1.2–6.1 eV, extending from the near-infrared to the ultraviolet. The measured ellipsometric parameters were analysed using a two-phase air/crystal model to derive the effective complex refractive index, dielectric function, absorption coefficient, optical conductivity, and the volume and surface energy-loss functions. All derived quantities are reported as pseudo-optical parameters due to the optical anisotropy of monoclinic $TlGaSe_2$ and the isotropic two-phase model employed. The resulting spectra reveal pronounced dispersion and absorption features associated with the fundamental absorption edge and higher-energy interband transitions. The fundamental absorption onset was located at approximately 2.02 eV from the first derivative of the pseudo-absorption coefficient and is consistent with independently determined band-gap values from transmission and reflection measurements. The below-edge pseudo-refractive-index dispersion was described by the Wemple–DiDomenico single-oscillator model, yielding physically consistent oscillator and static optical parameters. Complementary Raman measurements under two excitation wavelengths confirmed the characteristic intralayer vibrational modes at ∼131, ∼192, and ∼276 cm^{-1}. The results establish a self-consistent broadband optical dataset for $TlGaSe_2$.

1. Introduction

Thallium ternary chalcogenides $TlMeX_2$ (Me = Ga, In; X = S, Se) are layered semiconductors that have attracted sustained interest for optoelectronic and photodetector applications because of their strong optical anisotropy, near-visible band gaps and rich sequence of structural phase transitions [1, 2]. As with the isoelectronic III–VI layered chalcogenides GaSe and InSe, whose two-dimensional forms yield high-performance photodetectors [3, 4], $TlGaSe_2$ has been realised as an ultrathin phototransistor with broad-spectral photoresponse [5], as a visible-light thin-film photodetector [6] and, as a wide-band-gap thallium chalcogenide, has been explored for hard-radiation (x-ray and γ-ray) detection [7]. The family continues to yield photodetectors, most recently from solution-processed $TlInS_2$ nanoflake–polymer films reaching responsivities of 0.51 $A\,W^{-1}$ and detectivities above 10^{13} $cm\,Hz^{1/2}\,W^{-1}$ [8]. $TlGaSe_2$ crystallises in a monoclinic layered structure (space group $C2/c$ [9], with pseudo-tetragonal lattice parameters $a \simeq b \simeq 10.76$ Å, $c \simeq 15.62$ Å and $\beta \simeq 100°$ [10]). The layers are stacked along the c axis and held together by weak interlayer forces, so that the crystals cleave readily perpendicular to c and expose optically flat (001) surfaces that are well suited to reflection-based optical probes such as spectroscopic

© 2026 The Author(s). Published by IOP Publishing Ltd

ellipsometry (SE). The material is also a ferroelectric semiconductor that undergoes a sequence of structural (including incommensurate) phase transitions below room temperature [11–13], and its electronic structure, lattice dynamics and elastic response have recently been examined by first-principles methods [14–16].

The optical band gap of $TlGaSe_2$ has been reported repeatedly, with both indirect and direct edges typically placed close to 2 eV [1, 2, 17], and the near-band-edge emission and its anisotropy across the ferroelectric transition have been followed by photoluminescence and absorption measurements [18, 19]; the shape of the edge itself has been attributed to a Franz–Keldysh modulation of the absorption by the internal electric fields of charged native defects [20]. The dispersion of the refractive index and the single-oscillator (Wemple–DiDomenico) parameters have been examined for $TlGaSe_2$ and its layered analogues [21–23], while the dielectric function and interband transitions of the closely related compounds $TlGaS_2$ and TlInSeS have been mapped by SE [24, 25]. The same technique has recently been used to establish broadband reference optical constants for other layered chalcogenides, spanning 0.74–6.42 eV for GaSe [26], 300–3300 nm for SnS_2 and $SnSe_2$ [27], and the ultraviolet-to-near-infrared range for GeS_2 [28]. The first-order Raman spectrum has been characterised experimentally [9, 29] and modelled by first-principles lattice dynamics [15], and the dielectric and charge-transport behaviour of $TlGaSe_2$-based crystals has also been reported [10, 30]. Although the optical band edge and selected refractive-index parameters of $TlGaSe_2$ have been investigated by several techniques, a broadband and internally consistent description of its optical response across the transparent, band-edge, and strongly absorbing spectral regions remains limited. In particular, the earlier spectroscopic-ellipsometry study of $TlGaSe_2$ covered a comparable spectral range but was analysed only for above-band-gap critical points [31], and a more recent ellipsometric study of this compound was confined to the 320–850 nm window (about 1.5–3.9 eV) [11], whereas optical parameters reported in separate studies were obtained from different samples, spectral intervals, and analysis procedures. This fragmentation complicates direct comparison among the reported optical constants and limits their use in optical modelling and device-oriented calculations.

In the present work, the optical response of a freshly cleaved $TlGaSe_2$ single crystal is investigated continuously from the near-infrared to the ultraviolet over the photon-energy range of 1.2–6.1 eV. A mutually consistent set of effective pseudo-optical parameters, including the complex refractive index, dielectric function, absorption coefficient, optical conductivity and energy-loss functions, is derived from the same ellipsometric dataset. The fundamental absorption onset is evaluated using a derivative-based approach on the pseudo-absorption coefficient and cross-validated by Tauc analysis. The below-edge pseudo-refractive-index dispersion is analysed within the Wemple–DiDomenico single-oscillator framework. Complementary Raman measurements under two excitation wavelengths are used to verify the characteristic intralayer vibrational response and the reproducibility of the phonon positions. By integrating broadband ellipsometry, band-edge analysis, dispersion modelling, and vibrational characterisation within a single experimental framework, this study provides a consolidated pseudo-optical reference for $TlGaSe_2$.

2. Experimental details

$TlGaSe_2$ single crystals were grown by the Bridgman method, following the procedure described previously [32]. High-purity elements—gallium and selenium of 99.999% purity and thallium of 99.99% purity—were first reacted in stoichiometric proportion to synthesise polycrystalline $TlGaSe_2$, whose melting point is close to 817°C (1090 K). Single crystals were then grown from the stoichiometric melt sealed in an evacuated (10^{-5} Torr), carbon-coated silica ampoule (about 10 mm in diameter and 25 cm in length) tapered to a tip at the bottom. The ampoule was translated through a vertical furnace across a thermal gradient of $30\,^{\circ}\mathrm{C\,cm^{-1}}$ from 830 to 460°C at a rate of $1.0\ \mathrm{mm\,h^{-1}}$. The resulting dark-red ingot is stable in air and against moisture.

$TlGaSe_2$ crystallises in the monoclinic system and the structure is built from two-dimensional layers stacked perpendicular to the *c* axis, each successive layer being rotated by 90° about the stacking direction; the strong intralayer bonds are of Ga–Se character while the weaker interlayer coupling is mediated by Tl–Se bonds [9, 15]. Because of this layered habit the crystals cleave readily along the (001) plane, perpendicular to the *c* axis. Freshly cleaved platelets expose mirror-like (001) faces that require no further polishing or cleaning; such optically flat surfaces, ideal for reflection-based probes, were used as received for both the spectroscopic-ellipsometry and the Raman measurements. SE measurements were

performed at room temperature using a SOPRA GES-5E rotating-polariser ellipsometer over the photon-energy range of 1.2–6.1 eV with a spectral resolution of 0.01 eV. The measurements were carried out on freshly cleaved $TlGaSe_2$ crystal surfaces to obtain a smooth and contamination-free optical interface. To minimise possible surface oxidation and adsorption from the ambient atmosphere, the time interval between cleavage and data acquisition was kept below 15 min. The ellipsometric parameters Ψ and Δ, which describe the amplitude ratio and phase difference between the *p*- and *s*-polarised components of the reflected light, respectively, were recorded as functions of photon energy. The measurements were conducted at an angle of incidence of 70°. The pseudo-optical constants were extracted by direct two-phase (ambient/semi-infinite crystal) inversion of the measured Ψ and Δ at a single angle of incidence (70°). This inversion is a closed-form calculation with no adjustable parameters; consequently, no regression mean-square error, covariance matrix, or formal parameter uncertainties apply. To assess the reproducibility of the inversion, the raw $\tan\Psi$ and $\cos\Delta$ data were re-inverted independently in a separate computational environment (Python) and the results were compared with the original analysis; the agreement is reported in section 3.1. Because $TlGaSe_2$ is monoclinic and optically anisotropic, the quantities obtained from this isotropic two-phase model are effective pseudo-optical parameters representing the in-plane response of the (001) surface at $\phi = 70°$. Adding a surface-roughness or native-oxide layer to the model would require assumptions about layer thickness and composition that cannot be constrained from a single-angle measurement. The freshly cleaved surfaces were measured within 15 min of cleavage in ambient air to minimise surface contamination.

Raman spectra were recorded in back-scattering geometry at room temperature using a Renishaw confocal micro-Raman system with 532 nm and 785 nm laser excitation. The 532 nm channel employed a 1800-groove/mm grating and the 785 nm channel a 1200-groove/mm grating, both yielding a spectral resolution of approximately 1 cm^{-1}. The laser power at the sample was kept below 1 mW by applying a neutral-density filter to prevent local heating. Spectra were collected through 5× and 20× objectives, with acquisition times of 10–30 s per accumulation and three accumulations averaged per configuration. The wavenumber axis was calibrated against the 520.7 cm^{-1} line of a silicon standard before each measurement session. Each spectrum was corrected for cosmic-ray spikes with a Hampel filter, baseline-subtracted with an asymmetric least-squares algorithm, normalised to its strongest band and averaged over the repeats. Band positions and widths were obtained by fitting the averaged spectra to a sum of Lorentzian profiles via non-linear least squares; components whose width ran to the fitting bound with negligible amplitude were rejected as unconstrained. Fit uncertainties on peak centres range from ± 0.02 to ± 0.46 cm^{-1} depending on band intensity; the inter-excitation systematic offset ($+1.3 \pm 0.4$ cm^{-1}, section 3.6) is adopted as a conservative floor and all absolute positions are quoted to ± 1.5 cm^{-1}. The lowest recorded wavenumber was about 78 cm^{-1} for the 532 nm channel and about 100 cm^{-1} for the 785 nm channel, so the interlayer (rigid-layer) modes below these acquisition-window edges are not accessible in the present spectra; the mode census reported here is therefore restricted to the intralayer region above the cut-off.

3. Results and discussion

3.1. Pseudo-optical parameters and dielectric function

Figure 1 presents the experimentally measured ellipsometric parameters $\tan\Psi$ and $\cos\Delta$ of the $TlGaSe_2$ crystal as functions of photon energy. Both parameters exhibit pronounced spectral variations, particularly in the vicinity of 2.0–2.3 eV, indicating the onset of strong optical absorption associated with the fundamental interband transition. The oscillatory behaviour observed in $\cos\Delta$ below approximately 2.0 eV may be attributed to the relatively weak absorption and multiple-reflection effects occurring in the transparent spectral region. Above the absorption edge, $\tan\Psi$ increases progressively and reaches a broad maximum at approximately 5.3–5.6 eV, while the gradual variation of $\cos\Delta$ reveals additional spectral features that may be associated with higher-energy interband transitions. The optical response of $TlGaSe_2$ was evaluated using a two-phase air/sample optical model. The complex ellipsometric ratio was expressed as [31]

$$\rho = \frac{r_p}{r_s} = \tan\Psi \exp(i\Delta), \tag{1}$$

where r_p and r_s are the complex Fresnel reflection coefficients for the *p*- and *s*-polarised components of the incident light, respectively. Assuming the refractive index of air to be unity, the effective complex pseudo-dielectric function was calculated from

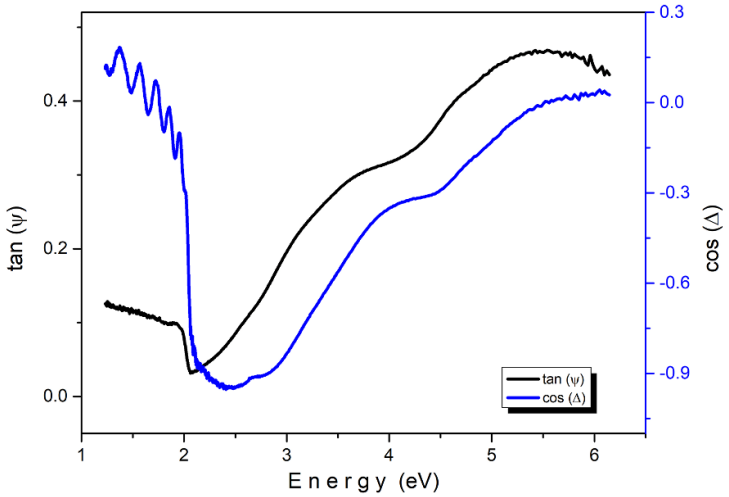

Figure 1. Experimentally measured ellipsometric parameters $\tan\Psi$ and $\cos\Delta$ of $TlGaSe_2$ as functions of photon energy.

$$\varepsilon = \varepsilon_1 + i\varepsilon_2 = \sin^2\phi\left[1 + \tan^2\phi\left(\frac{1-\rho}{1+\rho}\right)^2\right], \tag{2}$$

where ϕ is the angle of incidence. The pseudo-refractive index (n) and pseudo-extinction coefficient (k) were subsequently determined using

$$n = \left[\frac{\sqrt{\varepsilon_1^2+\varepsilon_2^2}+\varepsilon_1}{2}\right]^{1/2}, \tag{3}$$

and

$$k = \left[\frac{\sqrt{\varepsilon_1^2+\varepsilon_2^2}-\varepsilon_1}{2}\right]^{1/2}. \tag{4}$$

The remaining optical parameters were derived from the obtained n, k, ε_1, and ε_2 spectra using the corresponding standard optical relations. $TlGaSe_2$ crystallises in a monoclinic layered structure (space group $C2/c$) and is optically biaxial. However, light figure spectroscopy studies have demonstrated that the optical biaxiality of $TlGaSe_2$ at room temperature is very small [33]. Therefore, at room temperature, $TlGaSe_2$ can be regarded to a good approximation as a uniaxial material with its optic axis (c^*) oriented normal to the (001) layer plane [22, 31]. Because SE was conducted on cleaved (001) basal surfaces at an angle of incidence of $\phi = 70°$, the extracted quantities correspond to effective pseudo-optical parameters dominated by the in-plane dielectric response, rather than the fully resolved anisotropic dielectric tensor. Future studies employing generalised ellipsometry or multi-angle measurements would be necessary for a complete tensorial description.

Figure 2 shows the real and imaginary parts of the complex pseudo-refractive index of $TlGaSe_2$. The pseudo-refractive index n increases from approximately 2.6 at the low-energy limit to a maximum of about 3.6 near 3.0 eV, followed by a gradual decrease toward the ultraviolet region. This pronounced dispersion indicates a strong modification of the phase velocity and optical path length close to the interband-transition region. The pseudo-extinction coefficient k increases markedly above the fundamental absorption edge and reaches a broad maximum of approximately 1.8 near 4.7 eV. To verify the two-phase inversion, the raw $\tan\Psi$ and $\cos\Delta$ data were re-inverted independently in a separate computational environment using the same two-phase formula. The resulting n, k values agree with the original analysis to within root-mean-square deviations of $\Delta n_{rms} = 0.065$ and $\Delta k_{rms} = 0.076$ over the full 1.2–6.1 eV range, with the largest deviations confined to the strongly absorbing ultraviolet region where numerical sensitivity is highest.

The complex pseudo-dielectric function $\varepsilon = \varepsilon_1 + i\varepsilon_2$ is shown in figure 3. The real part ε_1 passes through a maximum of 12.5 at 2.97 eV and becomes small (and slightly negative) in the ultraviolet, while ε_2 peaks at 9.0 near 3.6 eV with a shoulder near 4.4 eV, reflecting the joint density of states of the interband transitions. The static (zero-frequency) pseudo-refractive index obtained below from the dispersion analysis, $n_0 = 2.45$, is consistent with the low-energy value of n in figure 2; it agrees with the

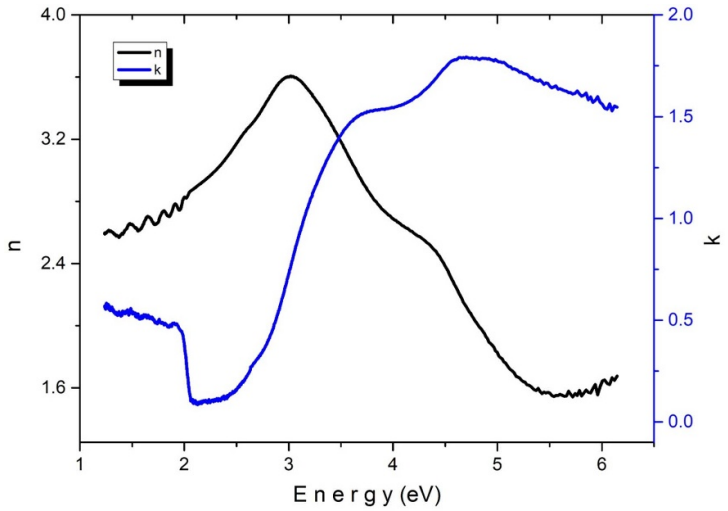

Figure 2. Pseudo-refractive index n (left axis) and pseudo-extinction coefficient k (right axis) of $TlGaSe_2$ as a function of photon energy.

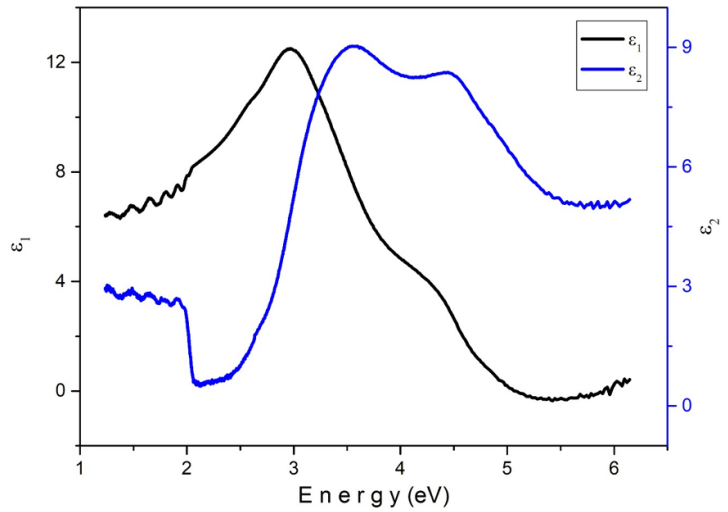

Figure 3. Real (ε_1, left axis) and imaginary (ε_2, right axis) parts of the pseudo-dielectric function of $TlGaSe_2$.

below-edge index $n(1.77\ \text{eV}) = 2.70$ [31] and lies above the ordinary-ray value $n_{so} \simeq 2.13$ [22]. The overall dielectric line shape—a rise to the main ε_1 maximum followed by a fall towards the ultraviolet, with ε_2 peaking above the gap—follows the profile obtained for $TlGaSe_2$ from first-principles calculations [34, 35], though direct quantitative comparison is limited by the pseudo-nature of the experimental data.

3.2. Absorption edge and band edge

The pseudo-absorption coefficient α (figure 4) reaches the true interband magnitude of $\sim 10^6$ cm^{-1} only above about 2.3 eV. Below 2 eV the two-phase inversion returns an inflated pseudo-absorption of order 10^4–10^5 cm^{-1}, which is an artefact of the semi-infinite model rather than genuine sub-gap absorption; across 2.0–2.1 eV this pseudo-absorption plateau collapses (α falling from $\sim 9 \times 10^4$ to $\sim 2 \times 10^4$ cm^{-1}). The fundamental absorption onset is located objectively from the minimum of the first derivative $\mathrm{d}\alpha/\mathrm{d}E$ (inset of figure 4), which coincides with this collapse and gives an onset energy of 2.02 ± 0.02 eV, the stated uncertainty reflecting the choice of derivative smoothing. The derivative minimum is a legitimate proxy for the edge because, below the true gap, the crystal is transparent and the spurious pseudo-absorption must fall away where genuine interband absorption begins; the located value therefore inherits the surface-model sensitivity of the pseudo-constants and is best regarded as an objective confirmation of the accepted $\sim$2 eV edge rather than a new determination. A weaker derivative maximum near 2.13 eV falls in the region where direct excitonic structure has been resolved in $TlGaSe_2$

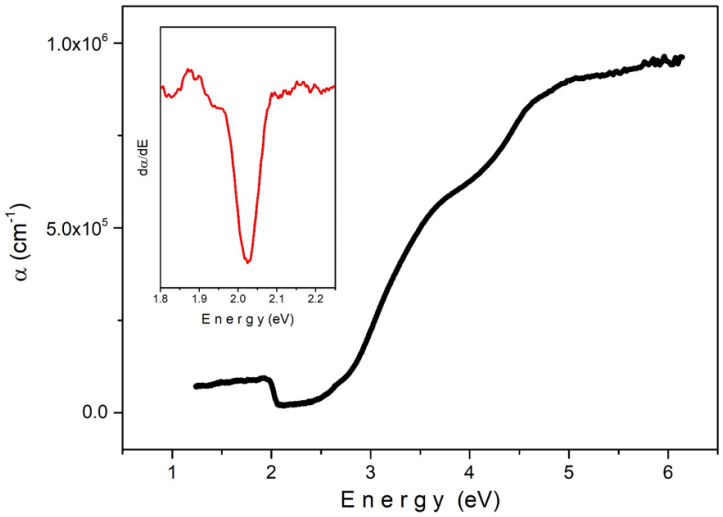

Figure 4. Pseudo-absorption coefficient α of $TlGaSe_2$. The inset shows the first derivative $d\alpha/dE$ near the edge; its minimum at 2.02 eV marks the fundamental absorption onset.

at low temperature, the direct excitonic absorption onset being placed at 2.127 eV at 15 K and shifting to lower energy on warming [1], consistent with the multi-edge picture of this material; in the isostructural sulfide $TlGaS_2$ the edge is likewise analysed in terms of both direct and indirect allowed transitions, with additional sub-band-gap radiative channels resolved by micro-photoluminescence [36]. The 2.02 eV feature falls within the band-edge energies reported for $TlGaSe_2$: it is close to the indirect Tauc gap of 2.02 eV [17] and to the direct photoconductivity gap of 2.04 ± 0.01 eV measured between 80 and 220 K [2], and lies just below the direct and indirect edges reported elsewhere [1, 19]. Because these are pseudo-optical constants, the derivative feature is best read as the fundamental absorption onset, not as a specific direct or indirect gap. To independently cross-validate this absorption onset, we refer to previous transmission and reflection measurements performed on $TlGaSe_2$ crystals from the same group [37], where standard Tauc analysis revealed the coexistence of an indirect band gap of $E_{gi} = 1.97$ eV and a lowest direct transition at $E_{gd} = 2.26$ eV at room temperature. The derivative onset obtained here (2.02 ± 0.02 eV) is in close agreement with this independently determined indirect gap (1.97 eV), confirming that the collapse of the sub-gap pseudo-absorption plateau marks the genuine interband absorption onset.

3.3. Pseudo-refractive-index dispersion (Wemple–DiDomenico)

In the weakly-absorbing region below and just above the edge (up to about 2.65 eV) the pseudo-refractive-index dispersion was analysed with the single-oscillator Wemple–DiDomenico model,

$$\frac{1}{n^2-1} = \frac{E_0}{E_\mathrm{d}} - \frac{1}{E_0 E_\mathrm{d}}(h\nu)^2, \tag{5}$$

in which E_0 is the single-oscillator energy and E_d the dispersion energy. Figure 5 shows $(n^2-1)^{-1}$ against $(h\nu)^2$ together with the linear fit ($R^2 = 0.977$). The slope and intercept give $E_0 = 3.76$ eV, $E_\mathrm{d} = 18.74$ eV, a static refractive index $n_0 = \sqrt{1 + E_\mathrm{d}/E_0} = 2.45$ and a static dielectric constant $\varepsilon_0 = n_0^2 = 5.98$. These single-oscillator parameters are window-dependent: restricting the fit to the fully transparent region ($h\nu < 1.9$ eV) instead gives $E_0 = 4.29$ eV, $E_\mathrm{d} = 22.3$ eV and $n_0 = 2.49$ ($R^2 = 0.78$), so the quoted E_0 should be read with this $\sim$15% spread in mind. The fitted quantity $(n^2-1)^{-1}$ uses only n and thus avoids the inflated below-edge pseudo-k, although the pseudo-n itself still carries the two-phase surface sensitivity; the near-exact below-edge n,k cross-check (root-mean-square $\sim$0.001) confirms that the inversion is at least reproducible there. The oscillator energy is close to the $E_0 = 3.16$ eV reported for the ordinary ray [22] and comparable to the $E_0 = 2.15$ eV obtained for $TlGaSe_2$ with a different fitting window [21], the dispersion energy $E_\mathrm{d} = 18.74$ eV being of the same order as the $E_\mathrm{d} = 13.82$ eV of that work [21]; the same single-oscillator treatment of transmittance and reflectance data gives $E_0 = 3.03$ eV and $E_\mathrm{d} = 17.35$ eV for undoped $TlInS_2$ [23]. Evaluated through $n_0 = \sqrt{1 + E_\mathrm{d}/E_0}$, these independent determinations correspond to static refractive indices of 2.73 for $TlGaSe_2$ [21] and 2.59 for $TlInS_2$ [23], and the long-wavelength ordinary refractive index of $TlGaSe_2$ obtained directly from reflection is 2.8 [38]; the present $n_0 = 2.45$ therefore lies below the 2.59–2.8 interval spanned by these independent

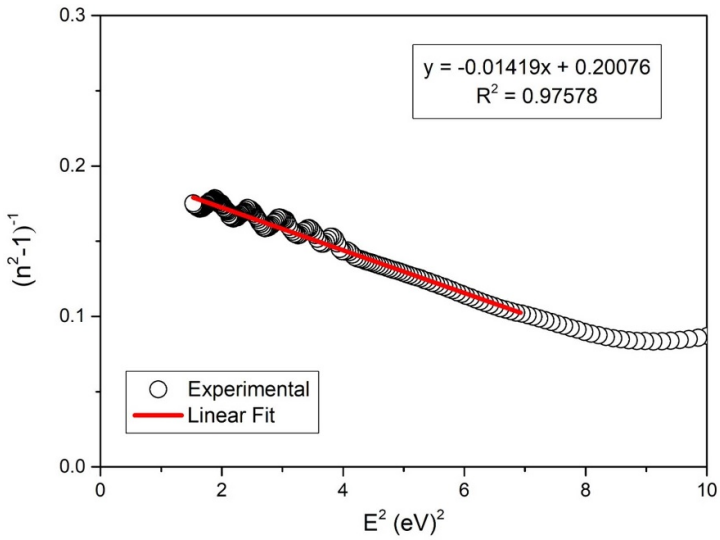

Figure 5. Wemple–DiDomenico plot of $(n^2-1)^{-1}$ against $(h\nu)^2$ for $TlGaSe_2$ in the weakly-absorbing region up to ~ 2.65 eV. The line is a least-squares fit to equation (5).

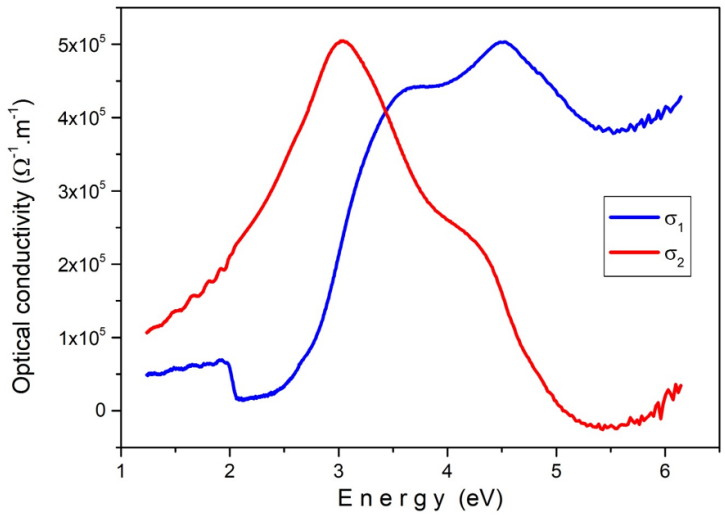

Figure 6. Real (σ_1) and imaginary (σ_2) parts of the pseudo-optical conductivity of $TlGaSe_2$.

determinations. The spread among these values reflects the different transparent windows and surface treatments rather than an intrinsic disagreement. The ratio E_0/E_g (1.86 for the wider window, 2.12 for the transparent-only fit, with $E_g = 2.02$ eV) is of the order expected for a single-oscillator description of a semiconductor, so the physical picture remains consistent across the window choices even though the specific E_0 is not.

3.4. Pseudo-optical conductivity

The complex pseudo-optical conductivity $\tilde{\sigma}(\omega) = \sigma_1(\omega) + i\sigma_2(\omega)$ was computed from the pseudo-dielectric function using the SI relation

$$\sigma_1(\omega) = \varepsilon_0 \omega \varepsilon_2(\omega), \qquad \sigma_2(\omega) = \varepsilon_0 \omega [1 - \varepsilon_1(\omega)], \tag{6}$$

where $\varepsilon_0 = 8.854 \times 10^{-12}$ F m^{-1} is the permittivity of free space and $\omega = E/\hbar$ is the angular frequency. The real and imaginary parts are shown in figure 6. σ_1 is small below the absorption edge, rises through the edge and exhibits a broad maximum of 5.0×10^5 Ω^{-1} m^{-1} near 4.5 eV, while σ_2 peaks at 5.0×10^5 Ω^{-1} m^{-1} near 3.0 eV. The onset of σ_1 coincides with the absorption edge, consistent with interband-transition-driven conductivity. The structure in σ_1 and ε_2 near 2.7–4.5 eV corresponds to the higher interband critical points of $TlGaSe_2$, placed at 2.75, 3.13, and 3.72 eV in earlier critical-point

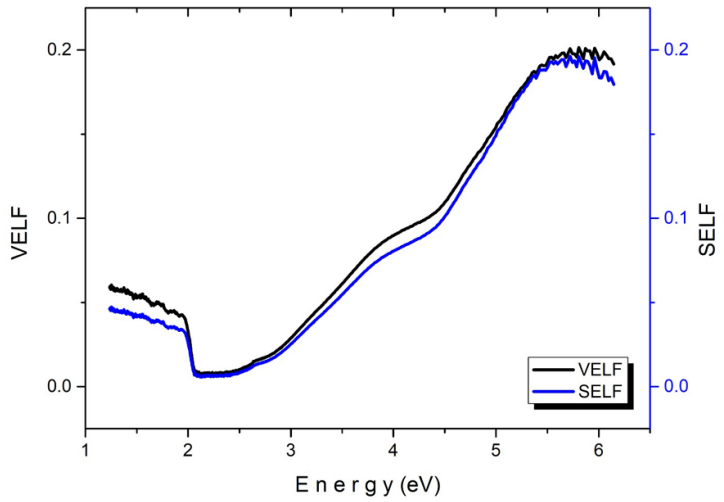

Figure 7. Volume (VELF) and surface (SELF) energy-loss functions of $TlGaSe_2$ as functions of photon energy.

analysis of dielectric function spectra [31] and consistent with first-principles band-structure calculations [34]. Because σ_1 and σ_2 are computed directly from ε_1 and ε_2 via equation (6), their spectral features represent internal self-consistency rather than independent experimental validation.

3.5. Energy-loss functions

The volume and surface energy-loss functions were computed from the pseudo-dielectric function as

$$\mathrm{VELF} = -\mathrm{Im}\left(\frac{1}{\tilde{\varepsilon}}\right) = \frac{\varepsilon_2}{\varepsilon_1^2+\varepsilon_2^2}, \qquad \mathrm{SELF} = -\mathrm{Im}\left(\frac{1}{\tilde{\varepsilon}+1}\right) = \frac{\varepsilon_2}{(\varepsilon_1+1)^2+\varepsilon_2^2}. \tag{7}$$

These functions describe the energy lost by a fast electron traversing the bulk and the surface of the crystal, respectively. Both are shown in figure 7. The two functions track one another closely, with VELF > SELF at every photon energy, as expected from the additional unity in the denominator of the surface term. Below the absorption edge both take small, slowly decreasing values (VELF falling from 0.059 at 1.24 eV to 0.033 at 2.0 eV); these below-edge magnitudes inherit the inflated pseudo-ε_2 of the two-phase inversion and should not be read as genuine sub-gap loss. Across 2.0–2.1 eV both functions collapse by a factor of about four to a common minimum of 0.007 (VELF) and 0.006 (SELF) at 2.13 eV, mirroring the collapse of the pseudo-absorption plateau at the same energy and marking the onset of genuine interband absorption. Above the edge both rise monotonically as interband transitions set in, reaching maxima of 0.20 at 5.81 eV (VELF) and 0.196 at 5.72 eV (SELF). No sharp plasmon resonance is resolved within the measured window: the loss functions are still broad and only weakly turning over at the high-energy limit, so the bulk plasmon energy of $TlGaSe_2$ lies at or above the 6.1 eV edge of the present measurement and is not determined here. As with the pseudo-optical conductivity, these quantities are derived from the same ε_1, ε_2 dataset and their spectral behaviour represents internal self-consistency rather than independent confirmation.

3.6. Raman scattering

The Raman spectra excited at 532 and 785 nm are compared in figure 8, and the multi-Lorentzian fit of the 532 nm spectrum is shown in figure 9. Above the low-wavenumber detection limit the spectra are dominated by three intralayer modes. Their fitted positions are 131.1, 192.2 and 275.8 cm^{-1} under 532 nm excitation and 132.4, 193.3 and 277.5 cm^{-1} under 785 nm excitation, the 192 cm^{-1} band being by far the strongest. Pairing the two excitations mode by mode gives a mean $785-532$ wavenumber difference of $+1.3\pm0.4$ cm^{-1}; all three pairs are positive, so this is a small *systematic* inter-channel offset rather than random scatter. Its root-mean-square value (1.4 cm^{-1}) is adopted as a conservative internal relative floor, and every absolute position is quoted to ±1.5 cm^{-1}; the agreement with independently published room-temperature positions to within 2.2 cm^{-1} (below) indicates the absolute axis is reliable at that level.

These frequencies are in good agreement with the literature. Resonance Raman scattering from $TlGaSe_2$ resolves intralayer modes in the same spectral region [9]. A pressure-dependent Raman study reports directly measured ambient-pressure room-temperature positions of 132, 177, 193, 229, 249 and

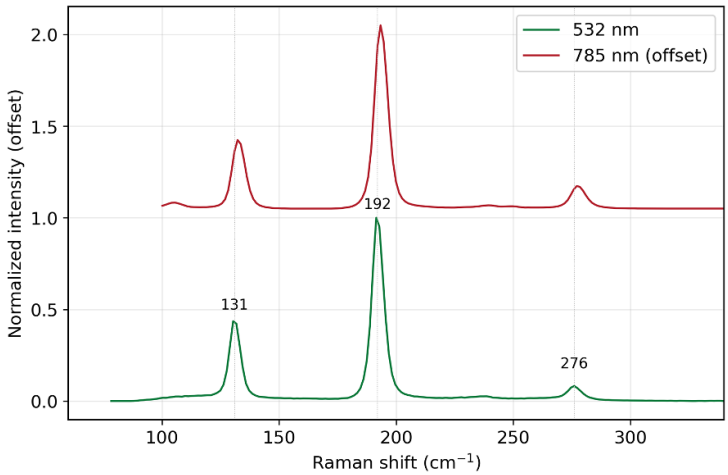

Figure 8. Room-temperature Raman spectra of $TlGaSe_2$ excited at 532 and 785 nm (the 785 nm spectrum is offset vertically for clarity). The dotted vertical lines mark the three intralayer modes discussed in the text.

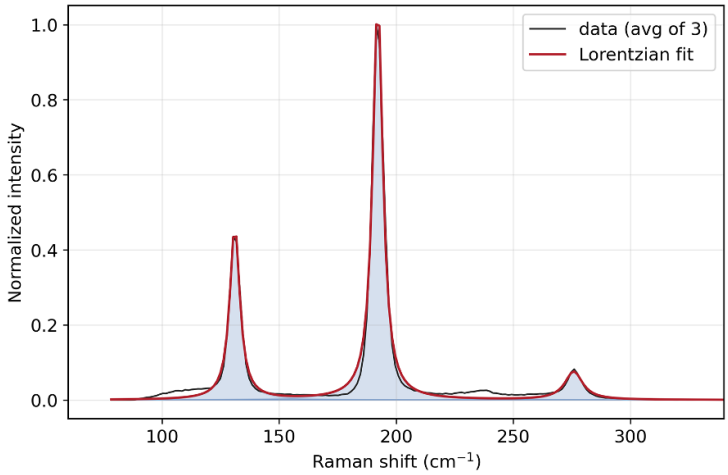

Figure 9. Multi-Lorentzian fit (red) of the averaged 532 nm Raman spectrum of $TlGaSe_2$ (black); the shaded curves are the individual Lorentzian components.

278 cm^{-1}, together with zero-pressure frequencies of 132.2 ± 0.4, 177.2 ± 0.5, 193.6 ± 0.3, 229.0 ± 0.1 and 277.7 ± 0.7 cm^{-1}, obtained by extrapolating a least-squares fit of the measured pressure dependence to zero pressure [39], and a later high-pressure study places two of the same modes at 193.4 and 275.4 cm^{-1} at ambient pressure [29]—so that the three positions reported here agree with these independent determinations to within 2.2 cm^{-1}, comparable to the ± 1.5 cm^{-1} floor adopted above. First-principles lattice-dynamics calculations likewise yield intralayer mode frequencies in the same range [15]. The three modes resolved here therefore coincide, within the calibration floor, with three of the characteristic intralayer modes of $TlGaSe_2$; the weaker bands near 177, 229 and 249 cm^{-1} [39] and the interlayer (rigid-layer) modes below the cut-off—which in the isostructural analogue $TlInS_2$ appear as distinct low-frequency features in polarised and low-temperature Raman spectra [40, 41]—are not resolved in the present spectra, so the mode census is bounded rather than complete. Group-theoretical analysis of the $C2/c$ structure predicts a large number of Raman-active modes ($23A_g + 25B_g$ at the zone centre) [15]; since the present measurement is unpolarised, a definite symmetry assignment cannot be made, but the dominance of the 192 cm^{-1} band is consistent with a totally symmetric (A_g-type) intralayer vibration, although a nearly degenerate B_g mode near 197 cm^{-1} [9] means the intensity alone cannot fix the symmetry.

4. Conclusion

The broadband optical response of layered $TlGaSe_2$ single crystals was investigated by spectroscopic ellipsometry (SE) over the 1.2–6.1 eV photon-energy range. The pseudo-optical parameters were derived using an isotropic two-phase air/crystal model applied to the (001) cleavage surface at $\phi = 70°$. The pseudo-refractive index ranges from approximately 2.6 in the near-infrared to a maximum of 3.6 near 3.0 eV, and the pseudo-extinction coefficient reaches a broad maximum of 1.8 near 4.7 eV. The real and imaginary parts of the pseudo-dielectric function reach maximum values of 12.5 (2.97 eV) and 9.0 (3.6 eV), respectively. The fundamental absorption onset was located at 2.02 ± 0.02 eV from the derivative of the pseudo-absorption coefficient, in agreement with the indirect band gap of 1.97 eV determined from transmission and reflection Tauc analysis and with band-edge values reported in the literature. The below-edge dispersion was described by the Wemple–DiDomenico model, yielding $E_0 = 3.76$ eV, $E_d = 18.74$ eV, $n_0 = 2.45$, and $\varepsilon_0 = 5.98$. The pseudo-optical conductivity and the volume and surface energy-loss functions, computed from the same dielectric dataset using SI relations, exhibit spectral features consistent with the absorption edge and higher-energy interband transitions. Complementary Raman measurements under 532 nm and 785 nm excitation resolved three intralayer modes at approximately 131, 192, and 276 cm^{-1}, with an inter-excitation reproducibility of ± 1.5 cm^{-1} and agreement with published values to within 2.2 cm^{-1}. The present results provide a continuous and internally consistent pseudo-optical dataset for $TlGaSe_2$. Resolution of the full anisotropic dielectric tensor would require generalised ellipsometry or multi-angle measurements and is identified as a direction for future work.

Data availability statement

The data cannot be made publicly available upon publication because no suitable repository exists for hosting data in this field of study. The data that support the findings of this study are available upon reasonable request from the authors.

Declaration of generative AI and AI-assisted technologies in the writing process

During the preparation of this work, the authors used large language models to improve language and readability. After using these tools, the authors reviewed and edited the content as needed and take full responsibility for the content of the publication.

Conflict of interest

The authors declare that they have no conflicts of interest.

Author contributions

Giray Mecit 0000-0002-8957-6545
Formal analysis (equal), Writing – original draft (equal)

Mehmet Isik 0000-0003-2119-8266
Conceptualization (equal), Methodology (equal), Writing – review & editing (equal)

Cansu Corapci 0009-0001-0742-3001
Formal analysis (equal)

Nizami Gasanly 0000-0002-3199-6686
Resources (equal), Supervision (equal), Writing – review & editing (equal)

References

[1] Grivickas V, Bikbajevas V and Grivickas P 2006 Indirect absorption edge of $TlGaSe_2$ crystals *Phys. Status Solidi b* **243** R31
[2] Özdemir S and Bucurgat M 2014 Photoelectrical properties of $TlGaSe_2$ single crystals *Solid State Sci.* **33** 25
[3] Sorifi S, Kaushik S and Singh R 2022 A GaSe/Si-based vertical 2D/3D heterojunction for high-performance self-driven photodetectors *Nanoscale Adv.* **4** 479

[4] Guo Z et al 2022 High-performance polarization-sensitive photodetectors on two-dimensional β-InSe Natl. Sci. Rev. 9 nwab098
[5] Yang S, Wu M, Wang H, Cai H, Huang L, Jiang C and Tongay S 2017 Ultrathin ternary semiconductor $TlGaSe_2$ phototransistors with broad-spectral response 2D Mater. 4 035021
[6] Ashraf I M, Shkir M, AlFaify S, Abdel-Wahab F, Ali A M, Sebak M A, Al-Juman M S A and Sanaa M F 2020 Development and characterization of $TlGaSe_2$ thin film-based photodetector for visible-light photodetector applications Opt. Mater. 103 109834
[7] Johnsen S et al 2011 Thallium chalcogenide-based wide-band-gap semiconductors: $TlGaSe_2$ for radiation detectors Chem. Mater. 23 3120
[8] Uçman Y K, Çetinkaya H G and Aydemir U 2025 Synthesis and photoelectric properties of $TlInS_2$ nanoflake-doped PVP thin-film photodetectors J. Mater. Sci.: Mater. Electron. 36 2081
[9] Syrbu N N, Tiron A V, Zalamai V V and Bejan N P 2017 Resonance Raman scattering in $TlGaSe_2$ crystals Adv. Condens. Matter Phys. 2017 5787821
[10] Asadov M M, Mustafaeva S N and Lukichev V F 2025 Frequency dispersion of dielectric coefficients in low-dimensional $TlGaSe_2$ and $TlInSe_2$ single crystals Russ. Microelectron. 54 1080–7
[11] Cengiz A, Gören S, Sönmez A, Şale Y, Okumuş E, Kırbaş C, Chumakov Y M and Seyidov M-H Y 2023 Modification of the optical and elastic properties of $TlGaSe_2$ layered semiconductor produced by the memory effect Phys. Scr. 98 125006
[12] Odrinskii A P 2020 Effect of modification of the contribution of the thermal emission of localized charges to the relaxation of the photoresponse of a $TlGaSe_2$ single crystal Phys. Solid State 62 682
[13] Molchanova A D, Asgarov K A and Allahverdiyev K R 2025 High-resolution optical spectroscopy of two-dimensional ferroelectric $TlGaSe_2$ in wide temperature range. New phase transitions? Physica B 712 417363
[14] Simonian T, Roy A, Bajaj A, Dong R, Lei Z, Sofer Z, Sanvito S and Nicolosi V 2025 Elucidating the role of stacking faults in $TlGaSe_2$ on its thermoelectric properties npj 2D Mater. Appl. 9 46
[15] Aliyeva V B, Jahangirli Z A, Ismayilova N A, Jabarov S H, Seyidov M-H Y and Mammadov T G 2026 First-principles calculations to investigate pressure-driven phase transition and elastic properties of $TlGaSe_2$ J. Sol-Gel Sci. Technol. 118 34
[16] Çaydaşı M, Mintaş M F, Chumakov Yu M, Volz S, Cengiz A and Seyidov M-H Y 2022 A study of thermoelectric performance of $TlGaSe_2$ layered dichalcogenides from first-principles calculations: vacancy defects modeling and engineering Phys. Status Solidi b 259 2100409
[17] Makhnovets G, Myronchuk G, Piskach L, Parasyuk O, Kityk I and Piasecki M 2018 Phase diagram and specific band gap features of novel $TlGaSe_2$:Zn^2+(Cd^{2+}, Hg^{2+})crystals J. Alloys Compd. 768 667
[18] Grivickas V, Gulbinas K, Gavryushin V, Bikbajevas V, Korolik O V, Mazanik A V and Fedotov A K 2014 Room-temperature photoluminescence in quasi-2D $TlGaSe_2$ and $TlInS_2$ semiconductors Phys. Status Solidi RRL 8 639
[19] Gulbinas K, Grivickas V and Gavryushin V 2014 Anisotropy of band gap absorption in $TlGaSe_2$ semiconductor by ferroelectric phase transformation Appl. Phys. Lett. 105 242107
[20] Gören S, Şale Y and Seyidov M-H Y 2024 The Franz–Keldysh effect in the optical absorption spectrum of a $TlGaSe_2$ layered semiconductor caused by charged native defects Semicond. Sci. Technol. 39 035008
[21] El-Nahass M M, Sallam M M, Rahman S A and Ibrahim E M 2006 Optical, electrical conduction and dielectric properties of $TlGaSe_2$ layered single crystal Solid State Sci. 8 488
[22] Shim Y G, Okada W, Wakita K and Mamedov N 2007 Refractive indices of layered semiconductor ferroelectrics $TlInS_2$, $TlGaS_2$ and $TlGaSe_2$ from ellipsometric measurements limited to only layer-plane surfaces J. Appl. Phys. 102 083537
[23] El-Nahass M M, Ali H A M and Abu-Samaha F S H 2013 Optical characteristics of $Tl_{0.995}Cu_{0.005}InS_2$ single crystals Physica B 415 57
[24] Kawabata T, Shim Y-G, Wakita K and Mamedov N 2014 Dielectric function spectra and inter-band optical transitions in $TlGaS_2$ Thin Solid Films 571 589
[25] Abdel-Wahab F, Ashraf I M, Shaltout A A, Badawi A, Ahmed S I and Hassan M E 2021 Ellipsometric study of the optical properties of TlInSeS layered crystal Opt. Mater. 114 110958
[26] Le L V, Nguyen T-T, Nguyen X A, Cuong D D, Nguyen T H, Nguyen V Q, Cho S, Kim Y D and Kim T J 2024 A systematic study of the temperature dependence of the dielectric function of GaSe uniaxial crystals from 27 to 300 K Nanomaterials 14 839
[27] Ermolaev G A et al 2022 Broadband optical constants and nonlinear properties of SnS_2 and $SnSe_2$ Nanomaterials 12 141
[28] Slavich A S et al 2025 Germanium disulfide as an alternative high refractive index and transparent material for UV-visible nanophotonics Light Sci. Appl. 14 213
[29] Jabarov S H, Aliyeva V B, Mammadov T G, Mammadov A I, Kichanov S E, Dubrovinsky L S, Babayev S S, Pashayeva E G and Dang N T 2018 High pressure Raman study of layered semiconductor $TlGaSe_2$ Mater. Sci.-Poland 36 203–8
[30] Asadov S M and Mustafaeva S N 2024 Effect of composition on charge transport in $(TlGaSe_2)_{1-x}(TlGaS_2)_x$ ($0 \leqslant x \leqslant 1$) solid solutions Inorg. Mater. 60 1283
[31] Isik M, Gasanly N M and Turan R 2012 Spectroscopic ellipsometry study of above-band gap optical constants of layered structured $TlGaSe_2$, $TlGaS_2$ and $TlInS_2$ single crystals Physica B 407 4193
[32] Isik M, Bulur E and Gasanly N M 2013 TL and TSC studies on $TlGaSe_2$ layered single crystals J. Lumin. 144 163
[33] Mamedov N, Shim Y and Yamamoto N 2002 Light figure spectroscopy of layered semiconductors Jpn. J. Appl. Phys. 41 7254
[34] Kharkhalis L Y, Glukhov K E, Babuka T Y and Liakh M V 2019 Band structures and optical properties related to substitutional impurities in $TlGaSe_2$ layered crystals: first-principles study Phase Trans. 92 451
[35] Benbahouche L, Khelefhoum A and Boucetta S 2024 Computational investigation of structural, electronic and optical properties of ternary chalcogenide $TlGaQ_2$ monoclinic compounds: a first-principles study Rev. Gest. Soc. Ambient. 18 e08033
[36] Bhattacharya S, Mondal S and Basak D 2025 Anomalous vibrational frequency shift and efficient radiative sub-band-gap electronic transitions in van der Waals quasi-2D post-transition-metal chalcogenide $TlGaS_2$ J. Phys. Chem. C 129 11012
[37] Gasanly N M 2010 Coexistence of indirect and direct optical transitions, refractive indices and oscillator parameters in layered $TlGaS_2$, $TlGaSe_2$ and $TlInS_2$ crystals J. Korean Phys. Soc. 57 164

[38] Kalomiros J A, Kalkan N, Hanias M, Anagnostopoulos A N and Kambas K 1995 Optical and photoelectric properties of $TlGaSe_2$ layered crystals *Solid State Commun.* **96** 601
[39] Henkel W, Hochheimer H D, Carlone C, Werner A, Ves S and von Schnering H G 1982 High-pressure Raman study of the ternary chalcogenides $TlGaS_2$, $TlGaSe_2$, $TlInS_2$ and $TlInSe_2$ *Phys. Rev. B* **26** 3211
[40] Paucar R, Shim Y-G, Mimura K, Wakita K, Alekperov O and Mamedov N 2017 Temperature dependence of low-frequency polarized Raman scattering spectra in $TlInS_2$ *Phys. Status Solidi c* **14** 1600214

[41] Gomonnai O O, Ludemann M, Gomonnai A V, Roman I Y, Slivka A G and Zahn D R T 2018 Low-temperature Raman studies of sulfur-rich TlIn(SSe) single crystals *Vib. Spectrosc.* **97** 114